



Provided by the author(s) and University College Dublin Library in accordance with publisher policies. Please cite the published version when available.

Title	Micro-Raman study of electronic properties of inversion domains in GaN-based lateral polarity heterostructures
Authors(s)	Park, M.; Cuomo, J. J.; Rodriguez, Brian J.; et al.
Publication date	2003-06
Publication information	Journal of Applied Physics, 93 (12): 9542-9547
Publisher	American Institute of Physics
Item record/more information	http://hdl.handle.net/10197/5372
Publisher's version (DOI)	10.1063/1.1570507

Downloaded 2022-08-25T19:22:00Z

The UCD community has made this article openly available. Please share how this access benefits you. Your story matters! (@ucd_oa)



Micro-Raman study of electronic properties of inversion domains in GaN-based lateral polarity heterostructures

M. Park^{a)} and J. J. Cuomo

Department of Materials Science and Engineering, North Carolina State University, Raleigh, North Carolina 27695

B. J. Rodriguez, W.-C. Yang, and R. J. Nemanich

Department of Physics, North Carolina State University, Raleigh, North Carolina 27695-8202

O. Ambacher

Center for Micro- and Nanotechnologies, Technical University Ilmenau, D-98693 Ilmenau, Germany

(Received 29 August 2002; accepted 7 March 2003)

The electronic properties of inversion domains in a GaN-based lateral polarity heterostructure were investigated using micro-Raman spectroscopy. The piezoelectric polarization of each domain was calculated from strain determined via Raman scattering. The free carrier concentration and electron mobility were deduced from the longitudinal optical phonon–plasmon coupled mode. The electron concentration in the N-face domain was slightly higher than that in the Ga-face domain. It appears that during growth, a larger number of donor impurities may have been incorporated into the N-face domain than into the Ga-face domain. © 2003 American Institute of Physics.

[DOI: 10.1063/1.1570507]

INTRODUCTION

Gallium nitride (GaN) has attracted significant attention due to its potential optoelectronic application in the short-wavelength optical spectral region. In the case of epitaxial GaN films, the [0001] direction of the GaN unit cell can be either parallel or antiparallel to the growth direction, resulting in domains with Ga-face or N-face polarity, respectively. Polarity can be controlled by the choice of substrate termination and/or the growth of nucleation layers.¹ Mixed polarity regions (inversion domains) can exist in GaN films, and these domains are separated by inversion domain boundaries.

Polarization in wurtzite GaN is attributed to spontaneous piezoelectric components. Spontaneous polarization (SP) originates from the intrinsic wurtzite crystal structure, whereas piezoelectric polarization (PZ) is induced by lattice distortion. The former is essentially independent of strain, while the latter originates from strain, which may be generated by lattice and/or thermal mismatch. Bernardini and Fiorentini² suggested that the value of the spontaneous polarization in GaN can be as high as 0.034 C/m². The strong built-in electric field generated by polarization can substantially affect the electrical and optical characteristics of a GaN-based heterostructure.³ For example, piezoelectric polarization in GaN/AlGaN quantum well structures can cause the separation of electrons and holes.⁴

It has been established that Raman spectroscopy can be employed for determination of the free carrier concentration and mobility in GaN. In polar semiconductors, longitudinal optical (LO) phonon modes couple strongly with plasmons through the macroscopic electric field.⁵ The coupling be-

tween the plasmon and the LO phonon produces two coupled LO phonon–plasmon (LPP) modes, ω_+ (LPP⁺) and ω_- (LPP⁻).⁶ The coupling is through the macroscopic electric fields of these excitations. The high frequency LPP⁺ mode behaves like a LO phonon at low carrier densities. The frequency of the LPP⁺ mode increases with the carrier concentration, and eventually corresponds to that of the plasmon. Such a mode was proposed by Varga,⁷ and observed in GaAs by Mooradian and Wright.⁶

Kozawa *et al.* have reported free carrier concentration determination by Raman scattering from analysis of the LO phonon–plasmon coupled mode in GaN.⁸ It was found that, as the electron concentration increases, the LO phonon couples with the overdamped plasmon, thereby shifting the $A_1(\text{LO})$ peak toward higher frequency and broadening the peak asymmetrically. Perlin *et al.* studied LO phonon–plasmon coupled modes in highly conducting bulk GaN.⁹ Both LPP⁺ and LPP⁻ modes were clearly observed in the Raman spectra and faithfully follow the theoretical trends. Contrary to Kozawa *et al.*'s report, evidence of overdamping behavior was not found, which may be attributed to the high quality single bulk crystalline samples (small needles or platelets).¹⁰ Harima *et al.* investigated underdamped LO phonon–plasmon coupled modes in *n*-type GaN.¹¹ They argued that the problem can be resolved by using high quality samples with moderate dopant concentrations (10^{17} – 10^{18} cm⁻³). Both the LPP⁺ and LPP⁻ modes were clearly identified in the Raman spectra. It was pointed out that plasmons in GaN behave like those in *n*-type GaAs since the degree of carrier damping in GaN is relatively small compared with that in other wide band gap semiconductors. In spite of these efforts, the degree of plasmon damping in GaN is still under debate.

^{a)} Author to whom correspondence should be addressed; electronic mail: m_park@ncsu.edu

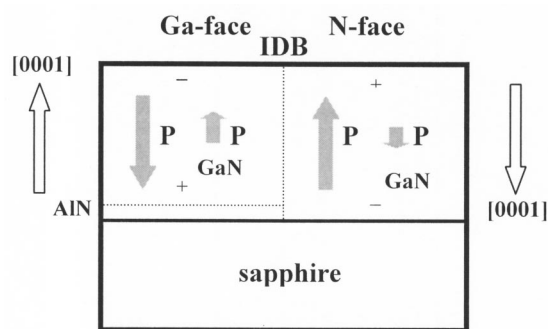


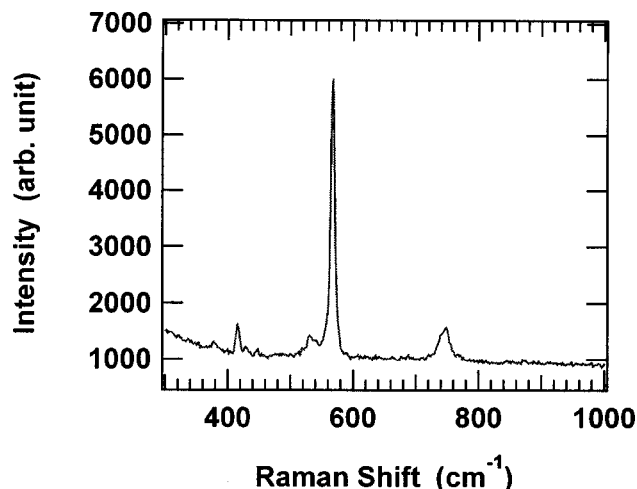
FIG. 1. Schematic cross section of the GaN-based lateral polarity heterostructure. The direction and magnitude of the spontaneous and piezoelectric polarization are depicted by the direction and length of the arrows, respectively.

Recently, Frayssinet *et al.*¹² presented evidence of a gradient in the free carrier concentration along the c axis in bulk GaN with high electron concentration. Infrared and Raman spectroscopy has revealed that the free electron concentration on the N face is higher than on the Ga face. They attribute this result to the preferential incorporation of oxygen impurities into the N face during growth. However, due to the nature of bulk crystal growth, anisotropy in processing including temperature and purity may result in variations during growth.

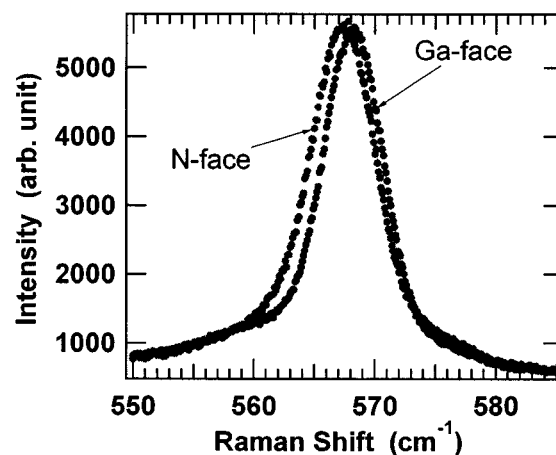
Therefore, in the present investigation, we have studied the electronic and piezoelectric characteristics of Ga- and N-face domains in a lateral polarity heterostructure using micro-Raman spectroscopy. Free carrier concentration, plasmon damping, free carrier mobility, and piezoelectric polarization (and total polarization) were determined from analysis of the Raman spectra. This work is different in that these parameters were obtained using an epitaxial film that contained opposite inversion domains, which were intentionally created at the same time with essentially identical processing conditions.

EXPERIMENT

The GaN-based lateral polarity heterostructure was fabricated using plasma-induced molecular beam epitaxy (PIMBE). The GaN epitaxial films were grown on a pre-patterned AlN/sapphire substrate. The Ga-face and N-face inversion domains were created on AlN/sapphire and sapphire regions, respectively. Details of the processing conditions are reported elsewhere.¹³ A schematic cross section of the structure is depicted in Fig. 1. Micro-Raman spectroscopy was carried out at room temperature using backscattering geometry with the 514.5 nm (2.41 eV) line of an Ar ion laser using an ISA U-1000 scanning double monochromator. The excitation laser beam was focused onto a small spot (2 μm in diameter) with a microscope objective. High resolution scans were obtained with 200 μm slit widths, resulting in 1.7 cm^{-1} instrumental resolution. The interval between the data points is 0.2 cm^{-1} . Survey scans were acquired using a 400 μm slit width and 2 cm^{-1} data interval [Fig. 2(a)].



(a)



(b)

FIG. 2. (a) Typical Raman spectrum of GaN-based lateral polarity heterostructure. (b) Raman spectrum of the $E_2^{(2)}$ peak of GaN (the Ga- and N-face regions).

RESULTS AND DISCUSSION

Hexagonal GaN has a wurtzite structure with a C_{6v}^4 space group and $A_1(z) + 2B_1 + E_1(x, y) + 2E_2$ optical modes at the Γ point of the Brillouin zone.¹⁴ The two E_2 modes are Raman active, the A_1 and E_1 modes are both Raman and infrared active, and the two B_1 modes are silent. Since the A_1 and E_1 modes are polar, they split into LO and transverse optical (TO) components. According to Raman selection rules, only the $E_2^{(1)}$, $E_2^{(2)}$, and $A_1(\text{LO})$ modes should be observed with the $z(-,-)z$ scattering geometry of our experiment.

Figure 2(a) shows a typical Raman spectrum of GaN. The sapphire E_g mode (at 748 cm^{-1}) was observed since GaN is transparent to the 514.5 nm line of the excitation laser. Raman spectra were collected at specific points across the inversion domain boundary from the N-face region to the Ga-face region. Figure 2(b) displays the Raman spectrum of

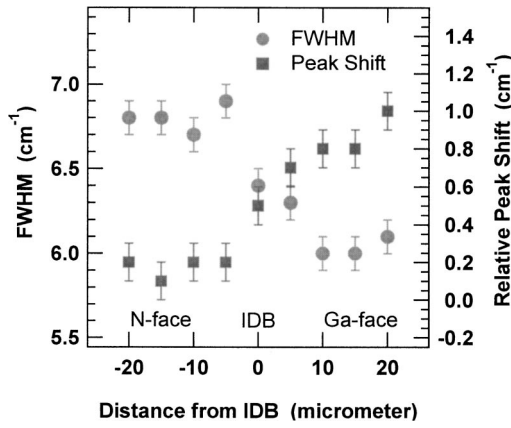


FIG. 3. Peak position and FWHM of the Raman $E_2^{(2)}$ mode determined by fitting the Raman peak with a Lorentzian function.

the $E_2^{(2)}$ peak of GaN (the Ga- and N-face regions). The peak position and full width at half maximum (FWHM) of the Raman $E_2^{(2)}$ mode were determined by fitting the Raman peak with a Lorentzian function, and the results are summarized in Fig. 3. The relative shift of the peak is the difference between the reference point and the observed peak position. We have used a value of 567.2 cm^{-1} as the reference point, which is the measured Raman peak position of the E_2 mode of a free-standing bulk GaN sample.

Kisielowski *et al.* found that biaxial stress of 1 GPa results in a shift of the $E_2^{(2)}$ Raman peak of GaN by $4.2 \pm 0.3 \text{ cm}^{-1}$.¹⁵ The positions of the Raman $E_2^{(2)}$ mode for the Ga-face and N-face domains were 568.0 and 567.4 cm^{-1} , respectively. This implies that the domains are under compressive stress. The calculated compressive stress on the Ga-face and N-face domains is 0.2 and 0.05 GPa, respectively, where 567.2 cm^{-1} was considered as the $E_2^{(2)}$ mode frequency of stress-free GaN. The Raman peak collected from the Ga-face domain is shifted by 0.65 cm^{-1} to higher wave number than that collected from the N-face region, indicating that the Ga-face domain exhibits 0.15 GPa larger compressive in-plane stress than the N-face domain.

Assuming that the hydrostatic stress contribution from point defects is negligible, two-dimensional biaxial stress can be considered to represent the state of residual stress of the thin film. The relation between stress and strain in the thin films can be expressed as

$$\varepsilon_a = E^{-1} \sigma_a (1 - \nu), \quad (1)$$

$$\varepsilon_c = -E^{-1} \sigma_a 2\nu, \quad (2)$$

where ε_a and ε_c are strain along the a and c axes, E is the Young's modulus, σ_a is the stress along the a axis (biaxial

stress, $\sigma_a = \sigma_b$, $\sigma_c = 0$), and ν is the Poisson ratio. Based on the Raman data and using Eq. (1), the in-plane biaxial compressive strain in the Ga- and N-face domains was calculated. The strain calculated in the Ga- and N-face domains is 4.0×10^{-4} and 1.0×10^{-4} , respectively. Piezoelectric polarization can be calculated using the following expression:

$$P_{\text{PZ}} = [e_{31} - (c_{13}/c_{33})e_{33}][2\varepsilon_a], \quad (3)$$

where e_{31} and e_{33} are piezoelectric constants, and c_{13} and c_{33} are the stiffness coefficients, which are listed in Table I. The calculated piezoelectric polarization in the Ga- and N-face domains is 4.1×10^{-4} and $1.0 \times 10^{-4} \text{ C/m}^2$, respectively. In the case of GaN under biaxial compressive stress, the directions of spontaneous and piezoelectric polarization oppose each other. Therefore, the total polarization ($P_{\text{Total}} = P_{\text{SP}} + P_{\text{PZ}}$) for the N-face domains has a slightly higher absolute magnitude than that for the Ga-face domains. Details of the direction and magnitude of the spontaneous and piezoelectric polarization are depicted in Fig. 1.

It should be noted that any measurement technique which can provide the value of strain can be used to provide a value of piezoelectric polarization. Previous measurements have established that Raman scattering and x-ray diffraction provide equivalent results on large area samples.¹⁶ In our samples with micrometer-sized patterned areas, micro-Raman spectroscopic determination of strain is more appropriate than x-ray diffraction due to its higher spatial resolution.

The FWHM of the $E_2^{(2)}$ Raman mode of the Ga-face domains is narrower than that of the N-face domains, which possibly implies a larger number of defects and impurities incorporated into the N-face domain. It is well known that the incorporation of impurities and point defects significantly reduces the phonon lifetime, thus broadening the Raman linewidth. Note that the Raman E_2 mode in GaN is not directly affected by variation in the free carrier concentration.

In GaN, where plasmon damping is significant, the LO phonon-plasmon coupling is displayed as a shift of the LO phonon mode. The plasma frequency can be deduced by fitting the coupled $A_1(\text{LO})$ phonon-plasmon peak to the following expression:¹⁷

$$I_A = \text{const} \cdot A(\omega) \cdot \text{Im}\{-\varepsilon(\omega)^{-1}\}, \quad (4)$$

where ω is the Raman shift, $\varepsilon(\omega)$ is the dielectric function, and $A(\omega)$ is related to the deformation-potential and the electro-optic mechanism. $A(\omega)$ is given by

TABLE I. Stiffness coefficients and piezoelectric coefficients of GaN.

	c_{11}	c_{12}	c_{13}	c_{33}	c_{44}	e_{31}	e_{33}
Stiffness coefficient ^a (GPa)	396	144	100	392	91		
Piezoelectric coefficient ^b (C/m ²)						-0.34	0.67

^aReference 34.

^bReference 35.

$$A(\omega) = 1 + 2C \frac{\omega_{\text{TO}}^2}{\delta} [\omega_p^2 \gamma (\omega_{\text{TO}}^2 - \omega^2) - \omega^2 \Gamma (\omega^2 + \gamma^2 - \omega_p^2)] + C^2 \{ \omega_p^2 [\gamma (\omega_{\text{LO}}^2 - \omega_{\text{TO}}^2) + \Gamma (\omega_p^2 - 2\omega^2)] + \omega^2 \Gamma (\omega^2 + \gamma^2) \} \times \left(\frac{\omega_{\text{TO}}^4}{\delta (\omega_{\text{LO}}^2 - \omega_{\text{TO}}^2)} \right), \quad (5)$$

where

$$\delta = \omega_p^2 \gamma \{ (\omega \Gamma)^2 + (\omega_{\text{TO}}^2 - \omega^2)^2 \} + \omega^2 \Gamma (\omega^2 + \gamma^2) (\omega_{\text{LO}}^2 - \omega_{\text{TO}}^2), \quad (6)$$

and C is the Faust–Henry coefficient,¹⁸ ω_p is the plasma frequency, ω_{TO} and ω_{LO} are the TO and LO phonon frequencies, respectively, and Γ and γ are the phonon and plasmon damping constants, respectively. The Faust–Henry coefficient can be deduced from the ratio of the intensity of the LO and TO phonon peaks in undoped GaN using the following equation:¹⁹

$$\frac{I_{\text{LO}}}{I_{\text{TO}}} = \left(\frac{\omega_0 + \omega_{\text{LO}}}{\omega_0 + \omega_{\text{TO}}} \right)^4 \frac{\omega_{\text{TO}}}{\omega_{\text{LO}}} \left\{ 1 + \frac{\omega_{\text{TO}}^2 - \omega_{\text{LO}}^2}{C \omega_{\text{TO}}^2} \right\}, \quad (7)$$

where ω_0 is the frequency of the laser. The dielectric function $\varepsilon(\omega)$ can be expressed as a combination of the contribution from phonons and plasmons,

$$\varepsilon(\omega) = \varepsilon_\infty \left(1 + \frac{\Omega^2}{\omega_{\text{TO}}^2 - \omega^2 - i\omega\Gamma} - \frac{\omega_p^2}{\omega(\omega + i\gamma)} \right), \quad (8)$$

where $\Omega^2 = \omega_{\text{LO}}^2 - \omega_{\text{TO}}^2$ and ε_∞ is the high frequency (optical) dielectric constant. From least square fitting, parameters ω_p , γ , Γ , and C can be obtained. If damping is neglected, the frequencies of the LPP⁺ and LPP⁻ modes can be calculated from

$$\omega_\pm^2 = \frac{\omega_{\text{LO}}^2 + \omega_p^2}{2} \pm \left[\left(\frac{\omega_{\text{LO}}^2 + \omega_p^2}{2} \right)^2 - \omega_p^2 \omega_{\text{TO}}^2 \right]^{1/2}. \quad (9)$$

Finally, the free carrier concentration (n) can be calculated using

$$\omega_p = \left(\frac{4\pi n e^2}{\varepsilon_\infty m^*} \right)^{1/2}, \quad (10)$$

where n is the free carrier concentration and m^* is the effective mass of the free carriers. The mobility of the free carrier can be obtained from

$$\gamma = \frac{e}{m^* \mu}. \quad (11)$$

Figure 4 shows Raman spectra in the region of the coupled $A_1(\text{LO})$ plasmon mode for the different polarity surfaces. The E_g mode due to the sapphire substrate is also observed. Each spectrum was fitted with two Lorentzian functions, and the results are summarized in Fig. 5. In the backscattering geometry from the (0001) surface, the $A_1(\text{LO})$ phonon mode propagates in the direction of the z axis, and the on-axis (z) electron mobility can be determined by the above-mentioned procedure. By using Eq. (9), the

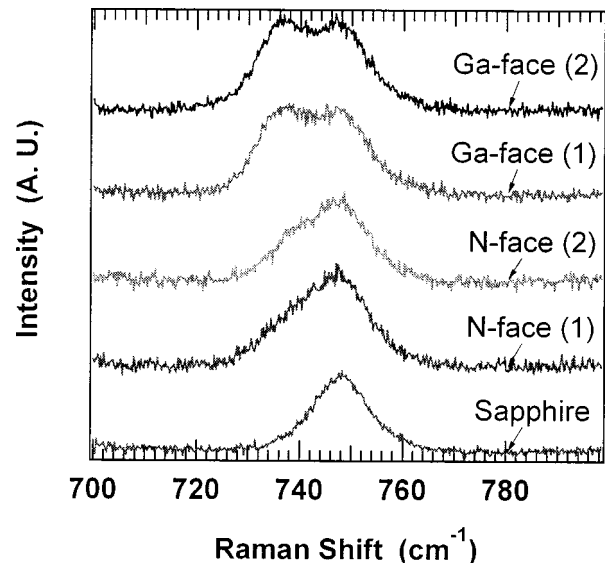


FIG. 4. Raman spectra of the $A_1(\text{LO})$ mode of GaN in the Ga- and N-face domains.

plasma frequency was calculated. The plasma frequency for the N-face region ($\omega_p = 135 \text{ cm}^{-1}$) was higher than that for the Ga-face region ($\omega_p = 96 \text{ cm}^{-1}$), which implies that the N-face domain has a higher free electron concentration than the Ga-face region. However, this is only an approximation since the LPP⁻ mode was not observed due to overdamping of the plasmon, i.e., the plasmon damping constant was larger than the plasma frequency ($\gamma > \omega_p$). Therefore, the peak was fitted with Eq. (1) after removing the sapphire substrate peak by spectral subtraction.

Figure 6 shows the experimental and theoretical line shape of the LPP mode as a function of the plasma fre-

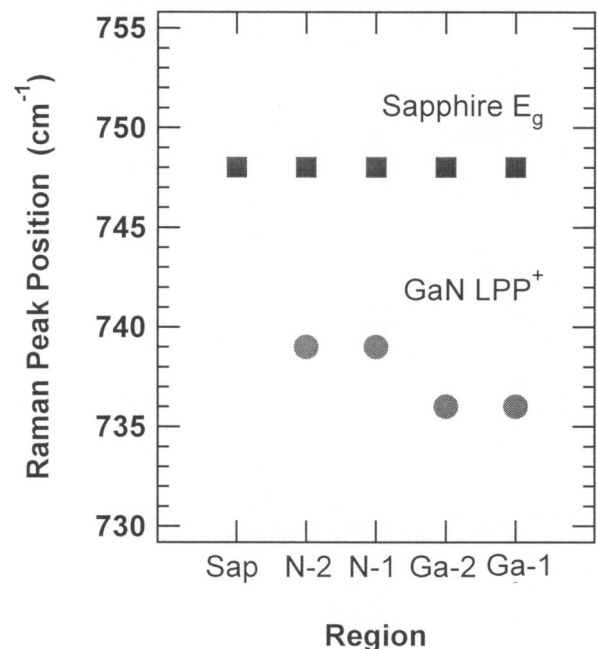


FIG. 5. Decomposed peak positions of the $A_1(\text{LO})$ mode of GaN and sapphire E_g mode.

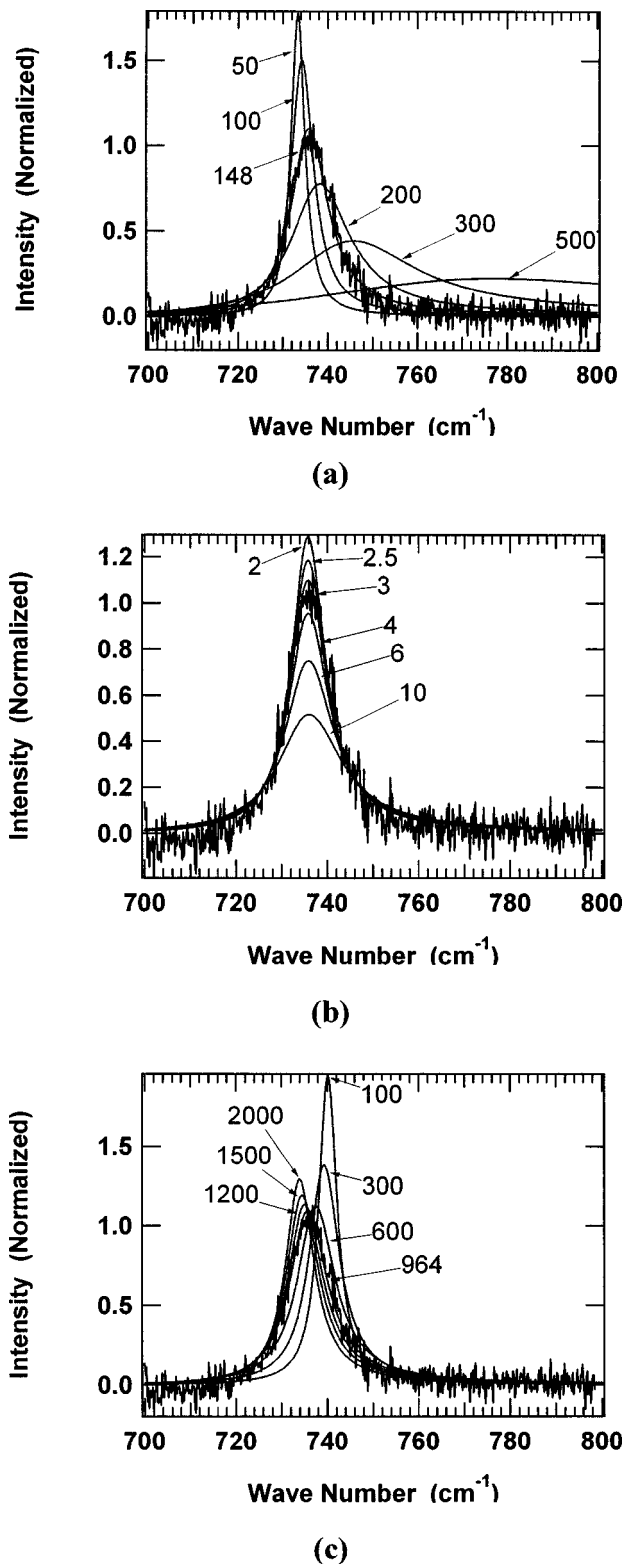


FIG. 6. Experimental and theoretical line shapes of the LPP mode as a function of the (a) plasma frequency, (b) phonon damping constant, and (c) plasmon damping constant.

quency, phonon damping constant, and plasmon damping constant. From line shape analysis, the plasma frequency, the phonon damping, and the plasmon damping constant were obtained. The free electron concentration and electron mobility were calculated using Eqs. (10) and (11), respectively.

The fixed value of the Faust–Henry coefficient ($C=0.4$) was used for this fit. The fitting results are summarized and tabulated in Table II. The results indicate that the free carrier concentration in the N-face domains is higher than that in the Ga-face domains.

According to the theoretical study by Zywieta *et al.*, the probability of incorporating donor impurities such as oxygen into N-face surfaces is higher than that into Ga-face surfaces.²⁰ This was experimentally observed by Frayssinet *et al.* in their infrared study.²¹ Due to the specific structural configuration of the Ga- and N-face sites, different affinity to oxygen may be expected. This is also supported by broadening of the E_2 mode in the N-face domain which can be attributed to the incorporation of impurities.

It should be noted that the $A_1(\text{LO})$ peak also shifts due to stress. It was reported that biaxial compressive stress of 1 GPa will shift the $A_1(\text{LO})$ peak toward a higher wave number by 0.8 cm^{-1} .²² Note that this is a factor of 5 less than the shift of the $E_2^{(2)}$ mode for the same biaxial stress. As was stated in the previous discussion, the Ga-face domains are 0.15 GPa more compressively stressed than N-face domains. Based on this difference in stress, the phonon frequency of the $A_1(\text{LO})$ mode of the Ga-face domains should be $\sim 0.1 \text{ cm}^{-1}$ higher than that of the N-face domains. This difference is negligible compared to the observed shift of $\sim 3 \text{ cm}^{-1}$. Therefore, we can safely disregard the effect of stress in our free carrier concentration determination.

Our measurement is different since the Ga- and N-face domains were formed at the same time on the same substrate using identical processing parameters. Therefore, the contrast manifested in the Raman spectra provides compelling evidence for this hypothesis. It appears that the incorporation of oxygen impurities into the N-face domains may relieve compressive stress originally produced by mismatch in the thermal expansion coefficients of GaN and sapphire. This is plausible since the atomic size of oxygen is smaller than that of nitrogen. Relaxation of residual stress with Si doping has previously been observed.²³ In this case, the smaller sized Si atoms replace the larger sized Ga atoms, resulting in the relaxation of the residual stress.

It should be noted that the value of the polarization induced charge is about $2 \times 10^{13} \text{ cm}^{-2}$. If the electron concentration is $> 2 \times 10^{17} \text{ cm}^{-3}$ and the GaN thickness is about $1 \mu\text{m}$, the electron sheet carrier concentration is equal to the polarization induced surface charge. In this case, the electric field induced by the piezoelectric and spontaneous polarization can be completely screened by the free electrons and ionized impurity atoms.

The electron mobility in the N-face domain was found to be higher than that in the Ga-face domain, and was manifested as larger plasmon damping in the Ga-face region. It is conjectured that the observed difference in plasmon damping is produced because of the difference in dislocation density. The dislocation densities for the Ga- and N-face domains are $\sim 8 \times 10^9$ and $\sim 1 \times 10^9 \text{ cm}^{-2}$, respectively.²⁴ It has long been considered that threading dislocations are electrically benign in GaN since they do not degrade the performance of GaN light emitting diodes.^{25,26} It was found from a transmission electron microscopy study that commercial blue light

TABLE II. Plasma frequencies, phonon damping constants, plasmon damping constants, Faust–Henry constants, free carrier concentration, and free carrier mobility obtained from line shape analysis.

	ω_p (cm^{-1})	Γ (cm^{-1})	γ (cm^{-1})	C	n_e (cm^{-3})	μ ($\text{cm}^2/\text{V s}$)
N face 1	185	3.3	813	0.4	3.9×10^{17}	60
N face 2	193	2.9	764	0.4	4.2×10^{17}	64
Ga face 1	146	3.2	912	0.4	2.4×10^{17}	54
Ga face 2	148	3.0	964	0.4	2.5×10^{17}	51

emitting diodes contain threading dislocation densities of $\sim 10^{10} \text{ cm}^{-2}$ in the active layer. In spite of this high dislocation density, a reasonable quantum efficiency and long lifetime have been obtained.^{27,28} However, recent studies by Rosner *et al.* show that electrically active threading dislocations do indeed affect the recombination characteristics in GaN.^{29,30} Threading dislocations act as nonradiative recombination centers in GaN and behave as deep level acceptors for *n*-type GaN. Coulomb scattering will occur since filled acceptor-like traps are negatively charged. It was argued that, in the case of low dopant concentrations, dislocation scattering dominates whereas impurity scattering becomes significant at high carrier concentration due to screening of the dislocation charge.^{31–33} Therefore, the slight difference in plasmon damping in the Ga- and N-face domains can be explained by differences in threading dislocation density.

SUMMARY AND CONCLUSIONS

Electronic properties of inversion domains in a GaN-based lateral polarity heterostructure were investigated using micro-Raman spectroscopy. The piezoelectric polarization of each domain was calculated from the strain determined by Raman spectroscopy. Free carrier concentrations and electron mobilities were deduced from analysis of the longitudinal optical phonon–plasmon coupled mode. The electron concentration in the N-face domains was slightly higher than that in the Ga-face domains. It appears that, during growth, a larger number of donor impurities may have been^{34,35} incorporated into the N-face domain than into the Ga-face domain.

ACKNOWLEDGMENT

This work was supported by the Office of Naval Research MURI on Polarization Electronics under Contract No. N00014-99-1-0729.

¹E. S. Hellman, MRS Internet J. Nitride Semicond. Res. **3**, 11 (1998).

²F. Bernardini and V. Fiorentini, Phys. Rev. B **64**, 085207 (2001).

³R. Dimitrov, A. Mitchell, L. Wittmer, O. Ambacher, M. Stutzmann, J. Hilsenbeck, and W. Rieger, Jpn. J. Appl. Phys., Part 1 **38**, 4962 (1999).

⁴T. Honda, T. Miyamoto, T. Sakaguchi, H. Kawanishi, F. Koyama, and K. Iga, J. Cryst. Growth **189/190**, 644 (1998).

⁵M. V. Klein, in *Light Scattering in Solids*, edited by M. Cardona (Springer, Berlin, 1975).

⁶A. Mooradian and G. B. Wright, Phys. Rev. Lett. **16**, 999 (1966).

⁷B. B. Varga, Phys. Rev. **137**, A1896 (1965).

⁸T. Kozawa, T. Kachi, H. Kano, Y. Taga, M. Hashimoto, N. Koide, and K. Manabe, J. Appl. Phys. **75**, 1098 (1994).

⁹P. Perlin, J. Camassel, W. Knap, T. Taliencio, J. C. Chervin, T. Susli, I. Grzegory, and S. Porowski, Appl. Phys. Lett. **67**, 2524 (1995).

¹⁰I. Grzegory and S. Krukowski, Phys. Scr., T **T39**, 242 (1911).

¹¹H. Harima, H. Sakashita, and S. Nakashima, Mater. Sci. Forum **264–268**, 1363 (1998).

¹²E. Frayssinet, W. Knap, S. Krukowski, P. Perlin, P. Wisniewski, T. Suski, I. Grzegory, and S. Porowski, J. Cryst. Growth **230**, 442 (2001).

¹³P. J. Schuck, M. D. Mason, R. D. Grober, O. Ambacher, A. P. Lima, C. Miskys, R. Dimitrov, and M. Stutzmann, Appl. Phys. Lett. **79**, 952 (2001).

¹⁴W. Hayes and R. Loudon, *Scattering of Light by Crystals* (Wiley, New York, 1978).

¹⁵C. Kisielowski, J. Krüger, S. Ruvimov, T. Suski, J. W. Ager III, E. Jones, Z. Liliental-Weber, M. Rubin, E. R. Weber, M. D. Bremster, and R. F. Davis, Phys. Rev. B **54**, 17745 (1996).

¹⁶L. T. Romano, C. G. Van de Walle, J. W. Ager III, W. Götz, and R. S. Kern, J. Appl. Phys. **87**, 7745 (2000).

¹⁷H. Yugami, S. Nakashima, and A. Mitsuishi, J. Appl. Phys. **61**, 354 (1987).

¹⁸W. L. Faust and C. H. Henry, Phys. Rev. Lett. **17**, 1265 (1966).

¹⁹M. Cardona, *Light Scattering in Solids II*, edited by M. Cardona and G. Güntherodt p. 61, (Springer, Berlin, 1982).

²⁰T. K. Zywiets, J. Neugebauer, and M. Scheffler, Appl. Phys. Lett. **74**, 1695 (1999).

²¹E. Frayssinet, W. Knap, P. Prystawko, M. Leszczynski, I. Grzegory, T. Suski, B. Beaumont, and P. Gibart, J. Cryst. Growth **218**, 161 (2000).

²²F. Demangeot, J. Frandon, M. A. Renucci, O. Briot, B. Gil, and R. L. Aulombard, Solid State Commun. **100**, 207 (1996).

²³I.-H. Lee, I.-H. Choi, C.-R. Lee, E.-j. Shin, D. Kim, S. K. Noh, S.-J. Son, K. Y. Lim, and H. J. Lee, J. Appl. Phys. **83**, 5787 (1998).

²⁴O. Ambacher (private communication).

²⁵S. D. Lester, F. A. Ponce, M. G. Craford, and D. A. Steigerwald, Appl. Phys. Lett. **66**, 1249 (1995).

²⁶L. Sugiura, J. Appl. Phys. **81**, 1633 (1997).

²⁷S. Nakamura, M. Senoh, N. Iwasa, S. Nagahama, T. Yamada, and T. Mukai, Jpn. J. Appl. Phys., Part 2 **34**, L1332 (1995).

²⁸S. Nakamura, M. Senoh, S. Nagahama, H. Iwasa, T. Yamada, T. Matushita, Y. Sugimoto, and H. Kiyoku, Appl. Phys. Lett. **70**, 1417 (1997).

²⁹S. J. Rosner, E. C. Carr, M. J. Ludowise, G. Girolami, and H. I. Erikson, Appl. Phys. Lett. **70**, 420 (1997).

³⁰S. J. Rosner *et al.*, Appl. Phys. Lett. **74**, 2035 (1999).

³¹N. G. Weimann, L. F. Eastman, D. Doppalapudi, H. M. Ng, and T. D. Moustakas, J. Appl. Phys. **83**, 3656 (1998).

³²H. M. Ng, D. Doppalapudi, T. D. Moustakas, N. G. Weimann, and L. F. Eastman, Appl. Phys. Lett. **73**, 821 (1998).

³³D. C. Look and J. R. Sizelove, Phys. Rev. Lett. **82**, 1237 (1999).

³⁴K. Kim, W. R. L. Lambrecht, and B. Segall, Phys. Rev. B **56**, 7018 (1997).

³⁵A. Zoroddu, F. Bernardini, P. Ruggerone, and V. Fiorentini, Phys. Rev. B **64**, 045208 (2001).